ARRAY ELEMENT LOCALIZATION OF A BOTTOM MOORED HYDROPHONE ARRAY

Matthew Barlee*, Stan Dosso*, and Philip Schey**
*School of Earth and Ocean Sciences, University of Victoria, Victoria BC V8W 3Y2
** Space and Naval Warfare Center (SPAWAR), 53560 Hull Street, San Diego, CA 92152-5001

ABSTRACT

In ocean acoustics, rapidly deployable, autonomous, bottom moored hydrophone arrays allow for quick, cost effective deployment, but result in poor knowledge of sensor positions. Because advanced array processing techniques, such as Matched Beam Processing, are highly sensitive to errors in sensor location, an accurate assessment of hydrophone positions is necessary. This paper discusses array element localization (AEL) and its use in localizing the ULITE array, a horizontal array deployed in the Timor Sea during the 1998 RDS-2 trial. The ill-posed inverse problem of determining source (imploded light bulbs) and receiver positions from the relative arrival times of source transients is solved through regularized linearized inversion. The inversion solution fits the data to high precision and provides individual hydrophone position estimates that provide the smoothest array shape that is consistent with the acoustic data.

RÉSUMÉ

Les systémes acoustiques marins qui sont rapidement deployés au fond de la mer, et qui fonctionnent avec autonomie, offrent une méthode de recherche qui est de faible cout, mais qui donne une pauvre connaissance de les positions des récepteurs. Pacreque la validité des manipulations des donnés, comme celles obtenues par le *Matched Beam Processing*, est fortement dépendente sur la location des instruments, une précise determination de la position de l'instrument est nécessaire. Ce papier décrit la méthode de Localization des Éléments d'Étalage (AEL) et son utilization dans la localization du systéme ULITE, un étalage horizontal déployé dans la mer de Timor pendant l'essai RDS-2 de l'an 1998. La question iverse mal posée, celle de la determination des positions de les sources (des ampoules implosées) et les récepteurs par les tems d'arivee relatifs des transients de source, est resolu par l'inversion linéale regularisée. La solution d'inversion est une excellente réprésentation de les donnés, et donne les positions de chaque hydrophone en accordance avec un model qui donne la forme optimale a l'étalage acoustique, et qui est consistent avec les donnés acoustiques.

1. INTRODUCTION

Accurate sound source localization in underwater environments has long proven to be a challenging but important endeavour. Modern developments in this field include the deployment and monitoring of large, autonomous bottom mounted vertical and/or horizontal hydrophone arrays. The benefit of this sensor autonomy comes at a cost—uncertainty in hydrophone location. Arrays are commonly deployed from surface vessels and lowered to depth, and as such, sea state, currents, and ship drift all combine to create uncertainty in the final resting position of each hydrophone.

Modern array processing techniques for source localization, such as matched field processing (MFP) and matched beam processing (MBP) involve correlating the received acoustic field with simulated fields computed using a numerical propagation model together with environmental parameters and source/receiver locations [1,2]. Receiver location errors have been shown to lead to significant degradation of both MFP and MBP performance [2], especially at higher frequencies (a commonly accepted rule suggests receiver positions must be known within $\lambda/10$, where λ is the wavelength at the frequency of interest, to achieve losses ≤ 1 dB in array processing [3]). As such, accurate array element location (AEL) is an important component of effectively processing acoustic field data. This paper will discuss the methodology and results of AEL for acoustic survey data collected for a bottom-moored, ultra-light (ULITE) horizontal array.

A common approach to AEL involves measuring arrival times of transient signals from controlled sources deployed around the array. Glass light bulbs mechan-

ically imploded at depth have proven to be a particularly useful sources due to their low cost, low environmental impact, and clean, repeatable signals [4]. If the source transmission instants and source positions are known and the ocean has a uniform (known) sound speed, the array elements can be located through a straightforward triangulation procedure. However, measuring source instants requires the sources and recording system be synchronized, which can be difficult and costly for at-sea deployments. Further, in practical AEL applications, the uncertainties in source positions are generally significant, and often represent the limiting factor in the accuracy of AEL inversion [5]–[7]. In addition, errors in the ocean sound speed can be significant: although measured sound-speed profiles are usually accurate in a relative sense, bias errors of up to 2 m/s due to imprecise calibration are not uncommon [8]. Finally, neglect of acoustic ray curvature due to refraction in a realistic, non-uniform ocean can also be a significant source of AEL error.

AEL represents a nonlinear inverse problem. Although such problems are sometimes treated as an optimization (i.e., determining the set of model parameters that minimizes the mismatch to measured data), a more complete approach to inversion involves determining the simplest solution that fits the measured data and *a priori* information to within their estimated uncertainties, together with an estimate of the uncertainties of the recovered parameters. A regularized AEL algorithm, based on iterated linearization, has recently been developed to accomplish this, and to treat the general case of ray-based inversion with unknown source instants, source positions, and sound-speed bias [5]–[7], [9],[10]. The regularized inversion yields the smoothest array shape (i.e., the shape with minimal curvature or changes in direction) that fits the acoustic data and prior position estimates to a statistically appropriate level. This minimum-structure solution includes all array-shape structure that is resolved by the data, but no structure that is unconstrained [5]. In contrast, minimizing the misfit often results in over-fitting data, introducing spurious (non-physical) structure into the model in an attempt to fit the noise on the data [5],[11]–[13]. The regularized approach is based on iterated linearized inversion, which provides an efficient AEL algorithm that is generally not sensitive to the initialization [5].

The translation of errors in the data, source positions and sound speed into errors in the sensor positions is determined by the AEL inverse problem; simple estimates based on forward calculations are not generally correct [7] (e.g., a 1-ms travel-time error in an ocean of sound-speed 1500 m/s does *not* imply a 1.5-m positioning error). Uncertainties in the recovered hydrophone positions are estimated here from the (linearized) model covariance matrix and through nonlinear Monte Carlo appraisal.

AEL has been carried out previously for the Timor Sea deployment of the ULITE array by the Defence Science and Technology Organization (DSTO) and the Space and Naval Warfare Systems Center (SPAWAR) [14]. The acoustic data were inverted by DSTO using simulated annealing optimization and by SPAWAR using the downhill simplex method [15]. In both cases source and hydrophone positions were treated as unknowns, although a uniform ocean with known sound speed was assumed and no uncertainty estimates were provided.

Following this introduction, the paper discusses the inverse and ray theory employed in the regularized linear inversion algorithm. Next, the RDS-2 experiment is described, followed by presentation of the UVic AEL solution for the ULITE array and a comparison with the DSTO and SPAWAR solutions. Finally, simulation is presented to demonstrate the sensitivity of matched beam processing to errors in array element location.

2. AEL INVERSION ALGORITHM

This section provides an overview of the inversion and ray theory which form the basis of the regularized AEL inversion algorithm. More complete treatments of AEL inversion can be found in [5]–[7],[9],[10], and of general inverse theory in [11]–[13].

2.1 Inverse Theory

The acoustic arrival times $\mathbf{t}$ measured in an AEL survey can be written in general vector form as

$$\mathbf{t} = \mathbf{T}(\mathbf{m}) + \mathbf{n}. \tag{1}$$

In (1), the forward mapping $\mathbf{T}$ represents computation of the travel times of acoustic signals along ray paths between sources and receivers (considered in Section 2.2). The model $\mathbf{m}$ of unknown parameters consists of three-dimensional (3-D) position variables (x, y, z) for each sensor, 3-D position variables and transmission instants for each source, and an unknown bias for the measured sound-speed profile. Finally, $\mathbf{n}$ represents additive errors (noise), with the assumption that the error n_i on datum t_i is due to an independent, Gaussian-distributed random process with zero mean and standard deviation σ_i.

The inverse problem of determining an estimate $\tilde{\mathbf{m}}$ of $\mathbf{m}$ is functionally nonlinear. However, a local linearization can be obtained by expanding $\mathbf{t}(\mathbf{m}) = \mathbf{t}(\mathbf{m_0} + \delta\mathbf{m})$ in a Taylor series to first order about an arbitrary starting model $\mathbf{m_0}$. Rearranging terms, this expansion can be written

$$\mathbf{J}\,\mathbf{m} = \mathbf{t} - \mathbf{t}(\mathbf{m_0}) + \mathbf{J}\,\mathbf{m_0} \equiv \mathbf{d}, \tag{2}$$

where $\mathbf{d}$ represents modified data defined in terms of known quantities and $\mathbf{J}$ is the Jacobian matrix of partial derivatives $J_{ij} = \partial T_i(\mathbf{m_0})/\partial m_j$ (given in Section 2.2). Equation (2) represents a linear inverse problem which can be solved for $\tilde{\mathbf{m}}$ as described below. Since nonlinear terms are neglected, the linearized inversion must be repeated iteratively until the solution converges.

The standard least-squares solution for linear inversion is determined by minimizing the χ^2 misfit

$$\chi^2 = |\mathbf{G}\,(\mathbf{J}\,\mathbf{m} - \mathbf{d})|^2 \tag{3}$$

with respect to $\mathbf{m}$, where $\mathbf{G} = \text{diag}[1/\sigma_i]$, with solution

$$\tilde{\mathbf{m}} = \left[\mathbf{J}^T\mathbf{G}^T\mathbf{G}\,\mathbf{J}\right]^{-1}\mathbf{J}^T\mathbf{G}^T\mathbf{G}\,\mathbf{d}. \quad (4)$$

However, treating both source and receiver positions as unknown leads to an ill-posed AEL inversion such that the matrix to be inverted in (4) is ill-conditioned. This ill-conditioning indicates that the data alone do not constrain the solution, and additional *a priori* information is required.

The method of regularization provides a powerful approach to include *a priori* information in linear inverse problems. This is accomplished by minimizing an objective function ϕ that combines the data misfit with regularizing terms that impose the prior information. Two forms of prior information are typically available in AEL problems, and can be imposed by including two regularization terms:

$$\phi = |\mathbf{G}\,(\mathbf{J}\,\mathbf{m}-\mathbf{d})|^2+\mu_1|\mathbf{H}_1\,(\mathbf{m}-\hat{\mathbf{m}}_1)|^2+\mu_2|\mathbf{H}_2\,(\mathbf{m}-\hat{\mathbf{m}}_2)|^2. \quad (5)$$

In (5), the first term represents the χ^2 data misfit, and the remaining terms represent regularizations (described below) with the variables μ_1 and μ_2 representing trade-off parameters (Lagrange multipliers) which determine the relative importance of the three terms in the minimization.

The first regularization term in (5) applies *a priori* parameter estimates for the source and receiver positions as available from the deployment procedure. Hence, $\hat{\mathbf{m}}_1$ consists of the prior estimates for these parameters and the regularization matrix $\mathbf{H}_1$ is of the form

$$\mathbf{H}_1 = \text{diag}[1/\xi_j], \quad (6)$$

where ξ_j represents the standard deviation of an assumed Gaussian uncertainty distribution for jth parameter estimate $\hat{m}_j$. The second regularization term applies the *a priori* expectation that the array shape is well approximated by a smooth function of an independent variable u, which can be applied using $\hat{\mathbf{m}}_2 = \mathbf{0}$ and $\mathbf{H}_2$ consisting of the tridiagonal matrix with nonzero entries on jth row given by

$$\mathbf{H}_2 = \text{tridiag}\left[\frac{-1}{(u_{j+1}-u_j)^2}, \frac{u_{j+2}-u_j}{(u_{j+2}-u_{j+1})(u_{j+1}-u_j)^2}, \frac{-1}{(u_{j+2}-u_{j+1})(u_{j+1}-u_j)}\right]. \quad (7)$$

Each row of $\mathbf{H}_2$ in (7) represents a discrete approximation to the second derivative operator $\partial^2/\partial u^2$. This regularization is applied to sensor positions along each segment of the array as a function of distance u along the segment. Hence, $|\mathbf{H}_2\,\mathbf{m}|^2$ provides a measure of the total curvature or roughness of the array shape, and the regularization produces the simplest array shape that is consistent with the acoustic data and prior position estimates. Since the smoothness term (7) depends on the prior information about the inter-sensor spacings, in cases where these are very poorly known, it may be preferable to omit this regularization to aid convergence.

The regularized solution is obtained by setting $\partial\phi/\partial\mathbf{m} = 0$, leading to

$$\mathbf{m} = \hat{\mathbf{m}}_1 + \left[\mathbf{J}^T\mathbf{G}^T\mathbf{G}\,\mathbf{J} + \mu_1\,\mathbf{H}_1^T\mathbf{H}_1 + \mu_2\,\mathbf{H}_2^T\mathbf{H}_2\right]^{-1} \cdot \left[\mathbf{J}^T\,\mathbf{G}^T\mathbf{G}\,\mathbf{d} - \mathbf{J}\hat{\mathbf{m}}_1\right]. \quad (8)$$

The regularization terms within the first set of brackets overcome ill-conditioning of the matrix, providing a well-posed inversion.

The implementation of the AEL inversion algorithm consists of an iterative application of the regularized solution (8), typically initiated from a starting model coinciding with the prior parameter estimates. Convergence of the algorithm is based on two criteria. First, the measured data must be fit to a statistically appropriate level such that the χ^2 misfit achieves its expected value of $\langle\chi^2\rangle = N$ for N data. Note that although (8) is derived based on the χ^2 misfit for the linear inverse problem, the convergence of the inversion algorithm must be judged in terms of the nonlinear misfit

$$\chi^2 = |\mathbf{G}(\mathbf{T}(\mathbf{m}) - \mathbf{t})|^2. \quad (9)$$

Second, a stable solution must be obtained such that the root-mean-square (RMS) change in the receiver positions between iterations is small compared to the expected accuracy of the solution (less than 0.1 m for the present application). A straightforward approach to assigning values to the trade-off parameters μ_1 and μ_2 to control the balance between the data misfit and *a priori* information leading to stable convergence is described in [5].

An important aspect of solving any inverse problem is to estimate the uncertainty of the solution. Two approaches are considered here. First, for linear inverse problems with Gaussian-distributed errors and prior estimates, the model covariance matrix is given by

$$\mathbf{C} = [\mathbf{J}^T\mathbf{G}^T\mathbf{G}\,\mathbf{J} + \mathbf{H}_1^T\,\mathbf{H}_1]^{-1}, \quad (10)$$

with the ith diagonal element of $\mathbf{C}$ representing the variance of the ith parameter $\tilde{m}_i$. For nonlinear inverse problems solved via iterated linearized inversion, the covariance matrix can be approximated by (10) with $\mathbf{J}$ evaluated at the final model solution. The validity of this approach depends on the degree of nonlinearity of the inverse problem, but has been found to be a good approximation for AEL inversion [7].

The second approach to parameter uncertainty estimation involves a Monte Carlo appraisal [5], [15]. In this procedure, the source and receiver positions determined via inversion of the measured data are assumed to define the true positions for a synthetic inverse problem, and acoustic arrival-time data are computed. A series of independent inversions are then carried out, each with different random errors applied to the computed data and to the prior position estimates and starting model (these errors are drawn from Gaussian distributions with standard deviations equivalent to

the corresponding estimated uncertainties of the data and prior). Standard deviations about the true sensor positions can then be computed from the ensemble of inversion results. Advantages of the Monte Carlo approach are that it represents a fully nonlinear analysis, and that uncertainties can be computed in an absolute or relative (sensor-to-sensor) sense. The disadvantage is increased computation time due to the multiple inversions.

Note that uncertainty estimation methods described above can be applied to predict AEL uncertainties for simulated cases in that they do not require measured data or prior estimates but only uncertainties for these quantities. Hence they provide a method to predict the localization accuracy for a particular scenario or to compare accuracies for different scenarios, as described in detail in [7]. This approach was used to consider the information content of surface-reflected arrivals as is discussed in Section 5.

2.2 Ray Theory

This section briefly describes the ray theory applied to compute the acoustic travel times and partial derivatives for the AEL inversion algorithm. Consider an acoustic source and receiver in the ocean at (x_j, y_j, z_j) and (x_i, y_i, z_i), respectively, with $z_j < z_i$ (source above receiver is assumed here with $z = 0$ at the surface and positive downward; for the reverse, a negative sign is required in all integrals below). The horizontal range between source and receiver is given by

$$r = \left[(x_i - x_j)^2 + (y_i - y_j)^2\right]^{1/2} . \qquad (11)$$

Expressions for the range r and arrival time T along a ray path between source and receiver follow from applying Snell's Law to an infinite stack of infinitesimal layers [14]

$$r = \int_{z_j}^{z_i} \frac{p\, c(z)\, dz}{\left[1 - p^2 c^2(z)\right]^{1/2}} , \qquad (12)$$

$$T = \tau + \int_{z_j}^{z_i} \frac{dz}{c(z)\left[1 - p^2 c^2(z)\right]^{1/2}} , \qquad (13)$$

where τ represents the source transmission instant and $c(z)$ the ocean sound speed profile. In (12) and (13), the ray parameter $p = \cos\theta(z)/c(z)$, derived from the grazing angle at the source, is constant along a ray path, and determining the correct value of p that connects source to receiver defines the take-off (grazing) angle at the source. The ray parameter for an eigenray connecting source and receiver is determined by searching for the value of p which produces the correct range using (12). An efficient procedure of determining p for direct-path eigenrays is based on Newton's method [5]. An initial estimate p_0 is calculated assuming straight-line propagation at the harmonic mean of the sound-speed profile between source and receiver

$$c_H = (z_i - z_j) \Big/ \int_{z_j}^{z_i} dz/c(z) . \qquad (14)$$

An improved estimate p_1 is obtained by expanding $r(p)$ in a Taylor's series about p_0 and neglecting nonlinear terms to give

$$p_1 = p_0 + \left[\frac{\partial r(p_0)}{\partial p}\right]^{-1} (r(p) - r(p_0)) . \qquad (15)$$

In (15), $\partial r/\partial p$ is determined by differentiating (12)

$$\frac{\partial r}{\partial p} = \int_{z_j}^{z_i} \frac{c(z)\, dz}{\left[1 - p^2 c^2(z)\right]^{3/2}} . \qquad (16)$$

If $r(p_1)$ computed from (12) is within the tolerance of the desired range, the procedure is complete. If not, the starting value is updated, $p_0 \leftarrow p_1$, and the procedure repeated iteratively until a satisfactory value is obtained.

In addition to travel times, the inversion algorithm requires partial derivatives of travel time with respect to source and receiver coordinates, source instant, and sound-speed bias. Consider first the partial derivative with respect to x_i. Employing the chain rule

$$\frac{\partial T}{\partial x_i} = \frac{\partial T}{\partial p}\frac{\partial p}{\partial r}\frac{\partial r}{\partial x_i} = \frac{\partial T}{\partial p}\left[\frac{\partial r}{\partial p}\right]^{-1}\frac{\partial r}{\partial x_i} . \qquad (17)$$

The three partials on the right side of (17) can be calculated from (13), (12) and (11), respectively, yielding

$$\frac{\partial T}{\partial x_i} = p\,(x_i - x_j)/r . \qquad (18)$$

Similar expressions are easily obtained for other horizontal derivatives. The partial derivative of T with respect to vertical coordinate z_i can be determined by differentiating (13) to give

$$\frac{\partial T}{\partial z_i} = \int_{z_j}^{z_i} \frac{p\, c(z)\, dz}{\left[1 - p^2 c^2(z)\right]^{3/2}}\frac{\partial p}{\partial z_i} - \frac{1}{c(z_i)\left[1 - p^2 c^2(z_i)\right]^{1/2}} . \qquad (19)$$

An expression for $\partial p/\partial z_i$ can be obtained by noting that

$$\frac{\partial r}{\partial z_i} = 0 = \int_{z_j}^{z_i} \frac{c(z)\, dz}{\left[1 - p^2 c^2(z)\right]^{3/2}}\frac{\partial p}{\partial z_i} - \frac{p\, c(z_i)}{\left[1 - p^2 c^2(z_i)\right]^{1/2}} . \qquad (20)$$

Solving for $\partial p/\partial z_i$ and substituting into (19) yields

$$\frac{\partial T}{\partial z_i} = \frac{1}{c(z_i)}\left[1 - p^2\, c^2(z_i)\right]^{1/2} , \qquad (21)$$

with a similar derivation for $\partial T/\partial z_j$. To account for bias in the measured sound-speed profile, let $c(z) = c_t(z) + c_b$, where $c_t(z)$ is the true sound speed and c_b is the bias. Differentiating (13) with respect to c_b leads to

$$\frac{\partial T}{\partial c_b} = -\int_{z_j}^{z_i} \frac{dz}{c^2(z)\left[1 - p^2 c^2(z)\right]^{1/2}} . \qquad (22)$$

Finally, the derivative of T with respect to the source instant τ in (13) is simply given by $\partial T/\partial \tau = 1$.

To implement the above equations, it is assumed that the measured sound-speed profile represents a series of layers with a linear sound-speed gradient in each layer. Sea surface or bottom reflections are modelled using the method of images, i.e., representing the reflected path by a direct ray path from an image source located above the surface or below the bottom, respectively. In the following, let $\{z_k, c_k\}$ represent the sound-speed profile, $\{c'_k\}$ be the corresponding sound speed gradients, and z_j and z_i be the source and receiver depths, respectively. The integrals in equations (12), (13), (16) and (22) can then be evaluated analytically as following, where $w_k \equiv (1 - p^2 c_k^2)^{1/2}$,

$$r = \sum_{k=j}^{i-1} \frac{w_k - w_{k+1}}{p\, c'_k}, \tag{23}$$

$$T = \tau + \sum_{k=j}^{i-1} \frac{1}{c'_k} \left[\log_e \frac{c_{k+1}\,(1 + w_k)}{c_k\,(1 + w_{k+1})} \right], \tag{24}$$

$$\frac{\partial r}{\partial p} = \sum_{k=j}^{i-1} \frac{w_k - w_{k+1}}{p^2\, c'_k\, w_k\, w_{k+1}}, \tag{25}$$

$$\frac{\partial T}{\partial c_b} = \sum_{k=j}^{i-1} \frac{1}{c'_k} \left[\frac{w_{k+1}}{c_{k+1}} - \frac{w_k}{c_k} \right]. \tag{26}$$

3. EXPERIMENT

In November, 1998, a multi-national experiment to study rapidly deployable systems, called RDS-2, was carried out to test and demonstrate advanced deployable array technologies, data recovery methods, and rapid array deployment techniques [16]. RDS-2 was conducted in the Timor Sea, 160 km west of Darwin, Australia. Bathymetry of the trial site indicates a very flat bottom (clay-sand with slope $\approx 0.1\%$) at 107 m depth.

The experiment employed three separate arrays, including an ultra-light horizontal array (ULITE) designed and deployed by SPAWAR. ULITE consists of three arms extending from a central node, each comprised of 32 hydrophone elements in three distinct 'nests' along its 470 m length. Element spacing was 7.8 m in the first nest, 15.6 m in the second, and 31.3 m in the third. The trial deployment plan involved fully extending each arm along radials separated by 120°, using three surface vessels to lower the array to the sea floor. However, high sea state, unequal cable tensions applied by the deployment vessels, and strong subsurface currents all conspired to produce an actual deployment pattern that is estimated to differ significantly from the intended array geometry (Fig. 1).

Prior estimates of hydrophone positions for the AEL inversion are chosen from the intended deployment pattern of the ULITE array. Due to poor control of the deployment procedure, a 5000 m horizontal uncertainty is assigned to the estimates of phone positions (essentially unconstrained) in the algorithm. Prior estimates of hydrophone depth are restricted to 107± 1 m, by virtue of the uniform bathymetry.

After array deployment, 23 light bulbs were lowered from a surface vessel and imploded at selected locations at an estimated depth of 52 m (Fig. 1). This source geometry was based on the intended array position. However, because of the disparity between intended and actual array positions, the source locations were less than ideal.

Bulb implosions were recorded at each hydrophone and relative travel times were determined by picking the time of the peak of the direct path arrival (Fig. 2). To increase the accuracy of picking peak arrivals, the digitally recorded data, sampled at 510.621 Hz, were upsampled by a factor of four. Subsequently, the highest interpolated point and it's two neighbours were then fit with a parabola, the peak of which was picked as the direct path arrival time. A data error of $\sigma = 0.5$ ms is assigned to arrival times for the inversion algorithm.

Prior estimates of the source positions are assigned the P-code GPS position of the Zodiac boat from which they were lowered. An x-y uncertainty of 10 m is assigned to account for GPS error and horizontal drift of the bulb at depth. The implosions were conducted over two different days, and although the sound speed profile did not differ appreciably, the very different surface conditions of those two days necessitated applying different vertical uncertainties to the sources for each day. Estimated depth of the first nine bulbs, imploded under higher seas, is 52±10 m, and the remain-

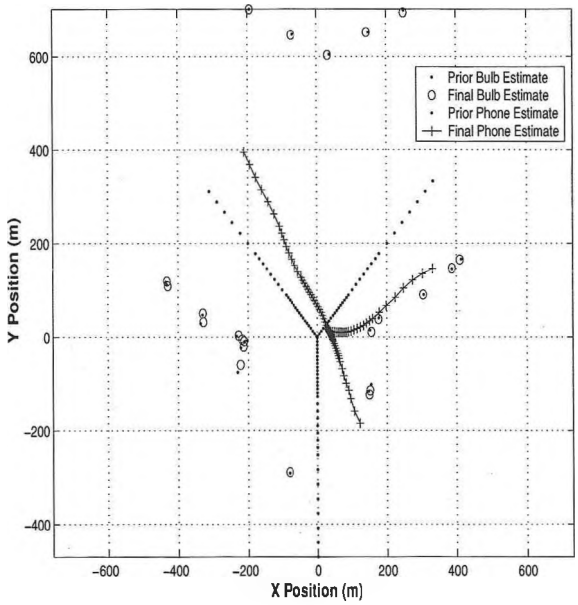

Fig. 1 Plan view of intended and recovered ULITE array positions including GPS fixed and recovered light bulb positions.

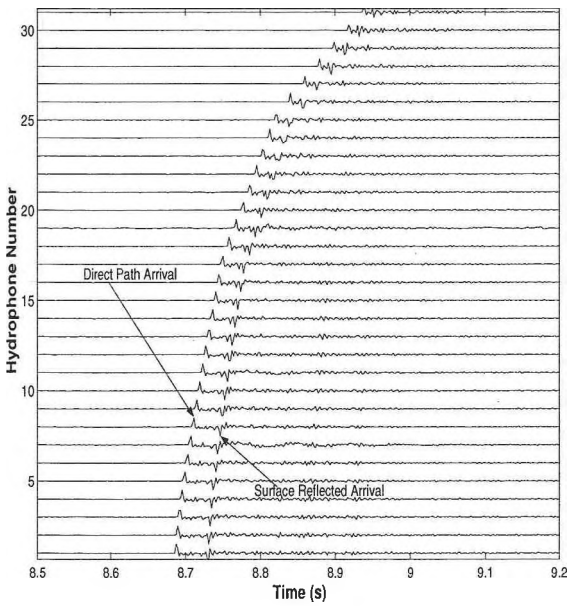

Fig. 2 Light bulb implosion acoustic arrivals for one arm (32 hydrophones) of ULITE array.

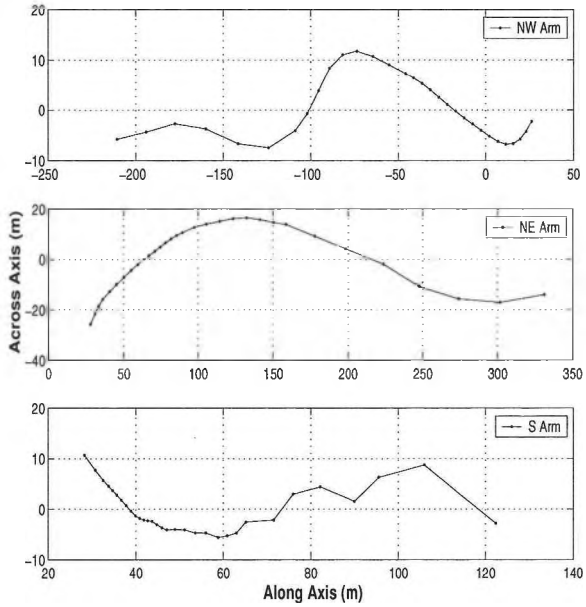

Fig. 3 Array structure shown in terms of the displacement from a straight line approximation of each arm.

der are assigned 52±5 m. Examination of the direct and surface reflected implosion arrivals reveals that the first three implosions were considerably shallower than planned, with the first implosion close to a depth of 30 m. Probable cause for this disparity is attributed to wind and swell conditions inducing significant drift of the Zodiac boat conducting the AEL survey. Because the implosions were so shallow, the arrivals of the direct and surface reflected signals overlap, resulting in the peak of the direct arrival being corrupted by the reflected arrival. For this reason, the first implosion is excluded from the AEL analysis. Fig. 2 illustrates the convergence of the two arrivals at longer ranges. Finally, a sound-speed bias uncertainty of 2 m/s was included.

4. RESULTS

4.1 Inversion Solution

The data set from the AEL survey consisted of 22 sources and 95 receivers (the end hydrophone of the NW arm was excluded due to movement caused by a tethered surface buoy), yielding $N = 2090$ equations for $M = 373$ unknowns from (12) and (13). Due to the large uncertainties of the hydrophone position prior estimates, five iterations were required to reduce the χ^2 misfit from the initial 18,484,570 to $N = 2090$, while concurrently decreasing the rms model change below the 0.1 m threshold. The result of the linearized inversion provides the simplest solution (*i.e.* minimal array structure), while fitting both the acoustic data and the prior estimates to a statistically appropriate level. A processing time of approximately 15 min was required to run the algorithm on a 400 MHz PC using a Unix OS.

The AEL inversion solution indicates that the actual position of the ULITE array was both shifted and rotated in relation to the planned layout. Prior receiver estimate residuals (the difference between prior estimates and recovered receiver positions) average 39.8 m in x, 88.1 m y, and 0.1 m in z. Maximum and minimum individual horizontal displacements of 310 m and 19 m are observed (Fig. 1). It appears that none of the three arms were fully extended to their 470 m length, with cumulative inter-element spacings totalling 440 m for the NW arm, 343 m for the NE arm, and only 225 m for the S arm. Fig. 3 depicts the structure in each arm as a function of element offset from a straight line (least squares) approximation to each arm. As expected from the short inter-element spacing, the south arm shows the most structure due to low cable tension during deployment.

Prior estimate residuals for source positions average 3.9 m in x, 3.4 m in y, and 1.7 m in z. As previously explained, the recovered positions of the first two implosions differ significantly from prior estimates, with vertical and horizontal displacements of approximately 20 m and 10 m, respectively. The recovered sound-speed bias of approximately 0.1 m/s was negligible.

4.2 Uncertainty Estimates

Absolute uncertainty estimates for receiver positions from both the linearized inversion and Monte Carlo appraisal, are presented in Fig. 4. Mean standard deviations of the linearized inversion solution are 2.4 m in x and y, and 0.6 m in z. Positional uncertainties increase

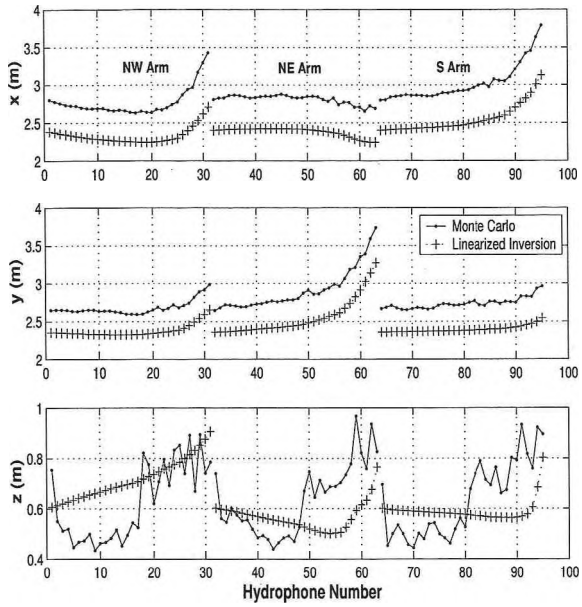

Fig. 4 Absolute hydrophone positional uncertainties using linearized inversion and Monte Carlo appraisal (one standard deviation).

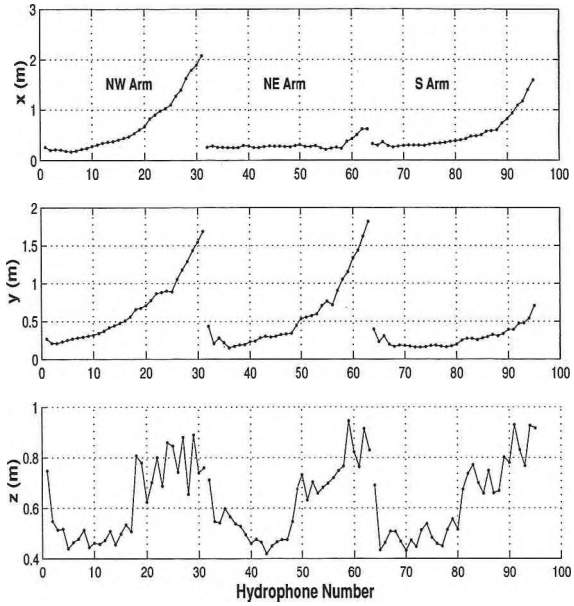

Fig. 5 Relative hydrophone positional uncertainties using Monte Carlo appraisal (one standard deviation).

towards the end of each arm due to the source-receiver geometry [7]. Linearized absolute uncertainties are in good agreement (< 20% difference) with those generated by a Monte Carlo appraisal involving 50 random realizations.

Fig. 5 shows the relative uncertainties in receiver position as estimated from the Monte Carlo appraisal. These values exclude translational errors of the entire array and represent the inter-element positional errors which severely impact acoustic field processing. The average standard deviation of these errors is 0.5 m in x and y, and 0.6 m in z, roughly equal to $\lambda/10$ at 250 Hz, the highest frequency used in MBP of the RDS-2 data.

5. AEL SOLUTION COMPARISONS

AEL for the ULITE array was previously conducted in independent studies by both SPAWAR and DSTO. This section presents a comparison of their results with the UVic AEL solution presented in this paper, as illustrated in Fig. 6.

SPAWAR used the same direct arrival time picks employed here, but assumed a constant sound velocity profile and straight line propagation. The inverse problem was solved using the downhill simplex method [15], which seeks to minimize travel-time errors through a series of geometric steps. A two-step inversion was applied. For the first step, source positions were fixed, providing a rough solution. The second step, using the rough solution as a starting model, allowed source movement in the final solution determination.

Using the method of simulated annealing [14],[15], DSTO sought to minimize error between modelled and actual arrival times for both direct-path and surface-reflection arrivals in a constant sound speed environment. To assess the value of including surface reflections in our method, we computed linearized sensor-position uncertainties for a case that included ideal surface reflections (eq. 10), and found only 10 cm and 20 cm improvement in horizontal and vertical standard deviations, respectively. The reason for such little improvement is that surface-reflected arrivals follow the same horizontal paths as the direct arrivals, and hence provide little new information in x and y [10], while the vertical position z is well constrained by the prior knowledge of water depth. Because of this and the fact that the observed direct/reflected arrival overlap at long ranges, we chose not to use reflected arrivals.

Fig. 6 presents the plan view of all three solutions, while Fig. 7 displays the x and y differences between the hydrophone positions. Examination of the figures reveals close similarity between the UVic and SPAWAR solutions with differences increasing towards the ends of the array arms to a maximum of 3.4 m in x and 2.6 m in y. Comparatively, larger differences are observed between the UVic and DSTO solutions. The DSTO solution appears shifted SW and rotated clockwise in relation to our array position, resulting in maximum x and y differences of 15.8 m and 14.5 m, respectively. As with the SPAWAR solution, DSTO element positions diverge from ours along the arms, and due to the apparent rotation about an axis near the array node, this divergence is amplified. Ref. 14 compares the DSTO solution with that achieved by

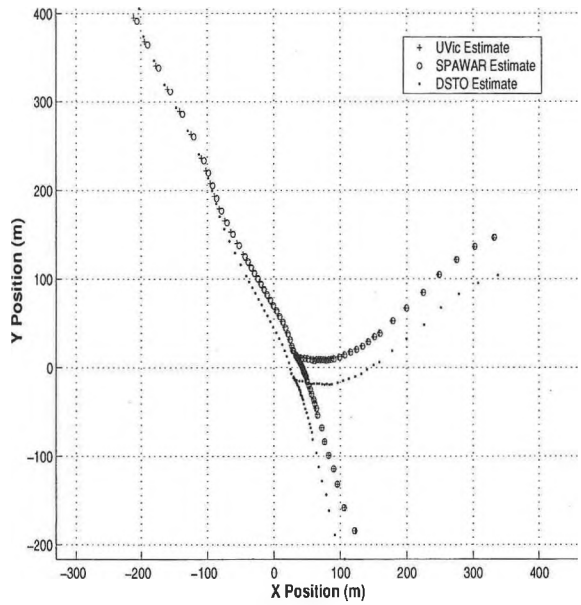

Fig. 6 Comparison of UVic, SPAWAR, and DSTO AEL solutions.

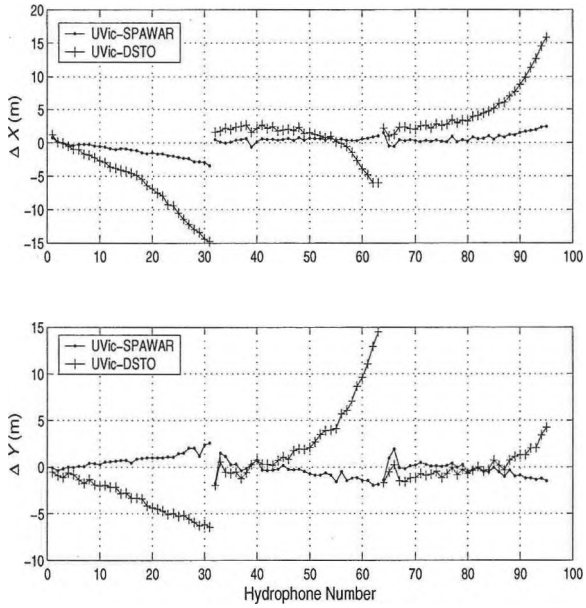

Fig. 7 Differences in relative sensor positions between UVic-SPAWAR and UVic-DSTO array estimates.

SPAWAR, attributing the shift and rotation to the use of large uncertainties allowed in the simulated annealing method. Additionally, DSTO's application of uniform, vice Gaussian uncertainties for prior position estimates allow a stronger influence from outliers.

Objective measures of the quality of an AEL solution involve assessing how well the solution fits the data and how smooth the solution is. On average, arrival time data were fit to within 0.38 ms for the UVic solution, 0.45 ms for the SPAWAR solution, and 0.90 ms for the DSTO solution. Array smoothness, or conversely structure, provides a measure of how simple a given solution to the problem is. Fig. 8 illustrates the structure in the S arm of the array as a function of hydrophone displacement from a straight line approximation to the respective solutions for the array arm. The DSTO solution can be seen to contain the most structure (e.g., zig-zags in the array shape), followed by the SPAWAR solution, while the UVic solution is the smoothest. Although not shown, solution smoothness was similar for the NE and NW arms, with DSTO showing the most structure and UVic the least.

6. AEL IMPACT ON SOURCE LOCALIZATION

To demonstrate the impact of inaccurate AEL, a example is presented in which MBP is applied to simulated receptions from the recovered positions of the NE and NW ULITE arms. For the simulation, a 200 Hz source is located at 50 m depth, 80° (ref. true north) from the ULITE node, at a range of 3 km. Simulated acoustic data was generated using the ORCA normal mode propagation model [17], to which Gaussian random errors were added resulting in a signal to noise ratio of 20 dB.

Fig. 9 depicts the range, bearing, and depth correlations between the simulated *true* model (receiver positions are exact), and *estimated* model in which Gaussian-distributed errors of specified standard deviations have been added to the receiver positions. For the first run (solid line), *estimated* receiver positions are the same as *true* positions, thus a high correlation (0.99) is achieved at the correct bearing, range, and depth. Random horizontal errors drawn from a Gaussian distribution with standard deviation equal to that of the relative errors for the AEL inversion are added to the *estimated* receiver positions for the second run (dashed line). The correlation is reduced slightly to 0.92 and the peaks remain at the correct bearing, range and depth. Doubling the standard deviation of the hydrophone perturbations begins producing range and depth estimation errors, and by the third run (dotted line) in which the standard deviation of induced errors is tripled ($\leq$ 7 m), significant degradation is seen in both range and depth. The source is falsely located at range 2.75 km and depth 10 m. Finally, using the prior hydrophone positional estimates in the MBP precluded any meaningful localization in range, bearing, or depth (not shown).

Simulations were also run using source frequencies of 50 and 100 Hz demonstrating that for lower frequencies, larger receiver positional errors are tolerated. For a 50 Hz source, errors on order of four standard deviations ($\leq$ 10 m) for the *estimated* model positions are tolerated by the matched beam processor before false maxima are observed in the correlation plots. Simi-

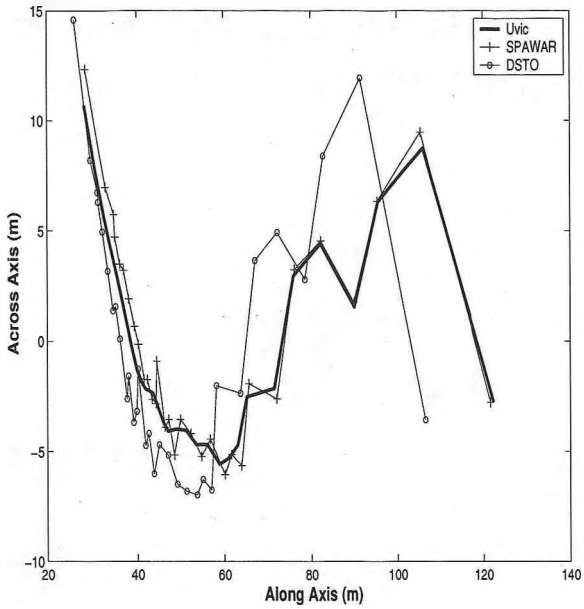

Fig. 8 Array structure of S arm in terms of displacement from straight line approximations of UVic, SPAWAR, and DSTO solutions

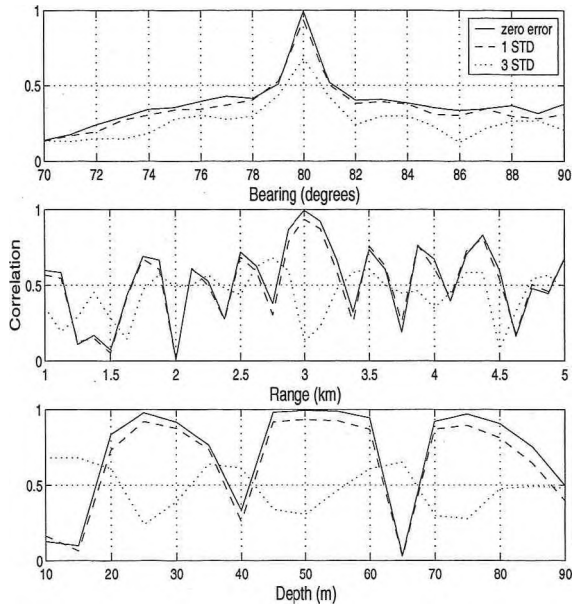

Fig. 9 MBP Simulation. Bearing, range, and depth correlations as a function of receiver positional error. Solid line represents zero error applied to estimated receiver positions; dotted and dashed lines represent errors of 1 and 3 standard deviations as estimated by the Monte Carlo appraisal.

larly, MBP of the 100 Hz fields begins showing false maxima with receiver perturbations of three standard deviations.

7. CONCLUSION

This paper demonstrates the application of regularized inversion in the challenging problem of accurately localizing the individual hydrophones of an autonomous, remotely deployed array. Due to complicating factors during array deployment in the RDS-2 trial, the final resting position of the ULITE array was virtually unknown. To localize the array, submerged light bulb implosions were conducted around the array and the relative arrival times of the transient signals were measured. Determining source and receiver positions from this data set represents an ill-conditioned inverse problem which is stabilized by assigning *a priori* estimates to source and receiver positions, and seeking the smoothest solution in the iterative linearized inversion algorithm. Relative element position errors are within acceptable ranges to allow subsequent source localization processing, with average standard deviations of 0.5 m horizontally and 0.6 m vertically.

8. ACKNOWLEDGEMENTS

The authors would like to thank Michael Greening and Jarrad Exelby of the Defense Science and Technology Organisation, Salisbury, S.A., Australia, for the valuable assistance and information provided. As well, a thank you to Michael Wilmut of UVic School of Earth and Ocean Sciences for his collaboration in the MBP simulation.

REFERENCES

[1] A. Tolstoy, 1993. *Matched-field processing for underwater acoustics*, World Scientific, Singapore.

[2] A. B. Baggeroer, W. A. Kuperman, P. N. Mikhalevsky, 1999. An Overview of Matched Field Methods in Ocean Acoustics. IEEE J.Ocean Eng., **18**,(4), 401–423.

[3] B. D. Steinberg, 1976. *Principles of Aperture and Array System Design.* Wiley, New York.

[4] G. J. Heard, M. McDonald, N. R. Chapman, 1997. Underwater Light Bulb Implosions: A useful Acoustic Source. Oceans 97. MTS/IEEE Conference Proceedings. IEEE Part 2, vol 2 755-762.

[5] S. E. Dosso, M. R. Fallat, B. J. Sotirin and J. L. Newton, 1998. Array element localization for horizontal
arrays via Occam's inversion. J. Acoust. Soc. Am., **104**, 846–859.

[6] S. E. Dosso, G. H. Brooke, S. J. Kilistoff, B. J. Sotirin, V. K. McDonald, M. F. Fallat, and N. E. Collison, 1998. High-precision array element localization of vertical line arrays in the Arctic Ocean. IEEE J. Ocean. Eng., **23**, 365–379.

[7] S. E. Dosso and B. J. Sotirin, 1999. Optimal array element localization. J. Acoust. Soc. Am. **106**, 3445–3459.

[8] H. T. Vincent II and S.-L. J. Hu, 1998. Geodetic position estimation of underwater acoustic sensors, J. Acoust. Soc. Am. **102**, 3099.

[9] S. E. Dosso and M. Riedel, 2001. Array element localization for marine seismic arrays. J. Acoust. Soc. Am. **110**, 955–966.

[10] S. E. Dosso and N. E. Collison, 2002. Acoustic tracking of a freely-drifting field of sonobuoys. J. Acoust. Soc. Am., **111**, 2166–2177.

[11] S. C. Constable, R. L. Parker, and C. G. Constable, 1987. Occam's inversion: A practical algorithm for generating smooth models from electromagnetic sounding data. Geophysics **52**, 289–300.

[12] W. Menke, 1989. *Geophysical Data Analysis: Discrete Inverse Theory* Academic Press.

[13] J. A. Scales, P. Docherty, and A. Gersztenkorn, 1990. Regularisation of nonlinear inverse problems: Imaging the near-surface weathering layer. Inverse Problems **6**, 115–131.

[14] M. V. Greening, 2000. Array element localization of rapidly deployed systems. Canadian Acoustics **28**,(2) 7–13.

[15] W. H. Press, B. P. Flannery, S. A. Teukolsky, and W. T. Vetterling, 1992. *Numerical Recipes.* Cambridge University Press, New York

[16] F. Desharnais, G. J. Heard, 1999. *TTCP Trial RDS-2: Rapidly Deployable Systems - Non-acoustic data* Technical Memorandum. Defense Research Establishment Atlantic, DREA TM 1999-069.

[17] E. K. Westwood, C. T. Tindle, N. R. Chapman 1996. A normal mode model for acousto-elastic ocean environments. J. Acoust. Soc. Am.**100**, 3631–3645.

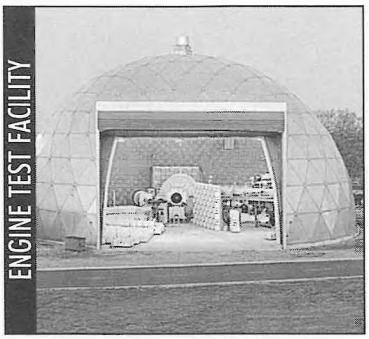

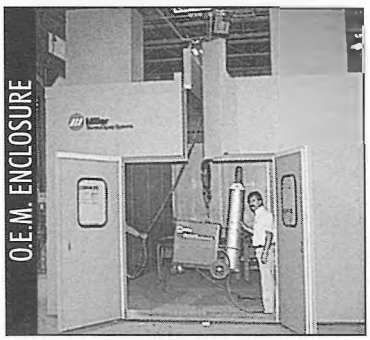

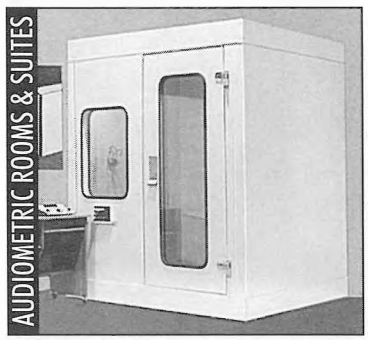

SOUND SOLUTIONS FOR THE FUTURE

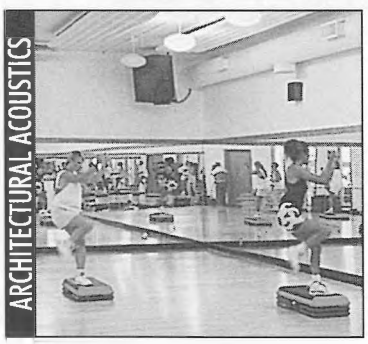

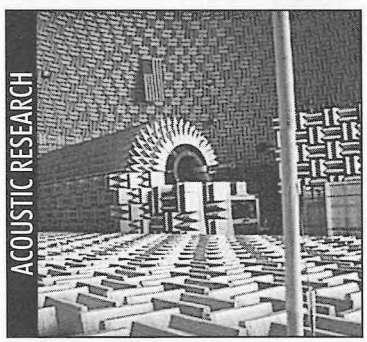

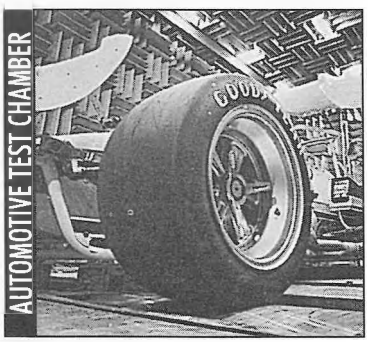

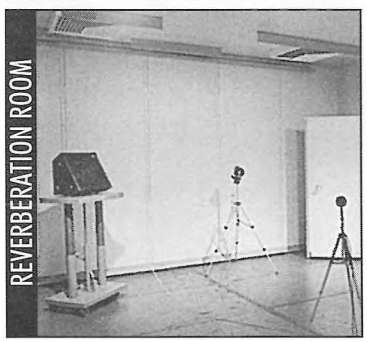

ECKEL

NOISE CONTROL TECHNOLOGIES

CANADIAN OFFICE
Box 776 100 Allison Avenue Morrisburg ON K0C 1X0
Tel: 613-543-2967 800-563-3574 Fax: 613-543-4173
Web site: www.eckel.ca/eckel e-mail: eckel@eckel.ca

NOISE CONTROL TECHNOLOGIES

Vibration Insulation

Regupol Regufoam

2 ways 1 goal

Rubber and foam products for optimal vibration absorption

Road Construction

Shock-proof and insulate in rail, tunnel, road and bridge construction.

- **Ballast Mats**

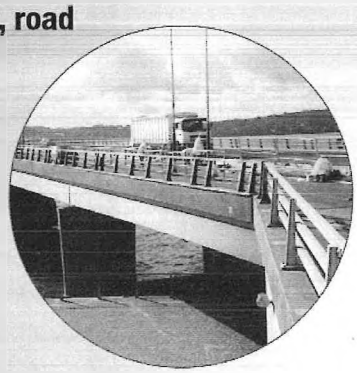

High-Rise Buildings

Provide vibration and impact sound insulation from mechanical equipment and foot fall noise.

- **Impact Sound Underlayment**

Foundations

Protect against ground vibration from subways and freight lines.

- **Bearing Pads**

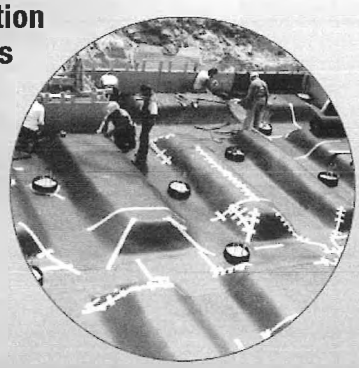

Industry

Insulate against rotating equipment and provide vibration insulation for sensitive equipment.

- **Floating Floors**

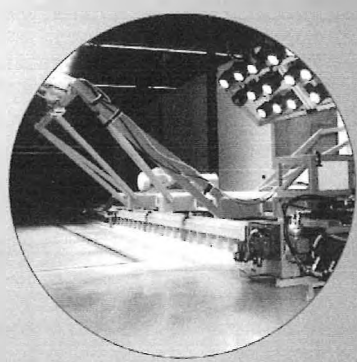

DODGE-REGUPOL
INCORPORATED

Leaders in recycled products technology

www.regupol.com

Phone: 416.440.1094
Toll free: **866.534.6086**

Fax: 416.440.0730
Email: pcd@regupol.com